Towards an Implantable Fluorescence Image Sensor for Real-Time Monitoring of Immune Response in Cancer Therapy

Rozhan Rabbani, Hossein Najafiaghdam, Mohammad Meraj Ghanbari, Efthymios P. Papageorgiou, Biqi Zhao, Micah Roschelle, Vladimir Stojanovic, Rikky Muller, and Mekhail Anwar

***Abstract*— Real-time monitoring of cellular-level changes inside the body provides key information regarding disease progression and therapy assessment for critical care including cancer therapy. Current state-of-the-art oncological imaging methods impose unnecessary latencies to detect small cell foci. Invasive methods such as biopsies, on the other hand, cause disruption if deployed on a repeated basis. Therefore, they are not practical for real-time assessments of the tumor tissue. This work presents a proof-of-concept design for an implantable fluorescence lensless image sensor to address the pervasive challenge of real-time tracking of the immune response in immunotherapy. The 2.4x4.7 mm^2 integrated circuit (IC) prototype consists of a 36 by 40 pixel array, a laser driver and a power management unit harvesting power and transferring 11.5 kbits/frame through a wireless ultrasound link while implanted 2 cm deep inside the body. Compared to prior art, this is the first full-fledged wireless system implementing chip-scale fluorescence microscopy to the best of our knowledge.**

***Clinical relevance*— This prototype can be used to personalize immunotherapy for the 50% of cancer patients who do not initially respond to the therapy.**

I. INTRODUCTION

Fluorescence microscopy is instrumental for obtaining cellular-level information from inside the body. One key application is real-time visualization of tumor response to therapeutic procedures to help oncologists assess effectiveness of the therapy during the course of the treatment. This is particularly relevant for immunotherapy, a game-changing therapeutic which exploits the immune system to attack cancer [1], but it is only effective in less than 50% of the patients [2], [3], [4], [5]. For patients who do respond, the immune system is unleashed to fight previously incurable cancers, resulting in long-term, durable responses [6]. For those who do not respond, detailed cellular-level information is needed to identify non-responders early on - when the window for cure is still viable - in order to quickly pivot and assess the response to additional therapies.

To date, this can only be accomplished by a biopsy and microscopic evaluation which is impractical on a repeated basis. Moreover, current imaging modalities cannot reveal real-time multicellular changes at micron-scale, instead relying on centimeter-scale growth to detect a change. Due to the latency and low sensitivity of the state-of-the-art imaging systems, the curative window is lost before a critical change in the tumor size is registered [7].

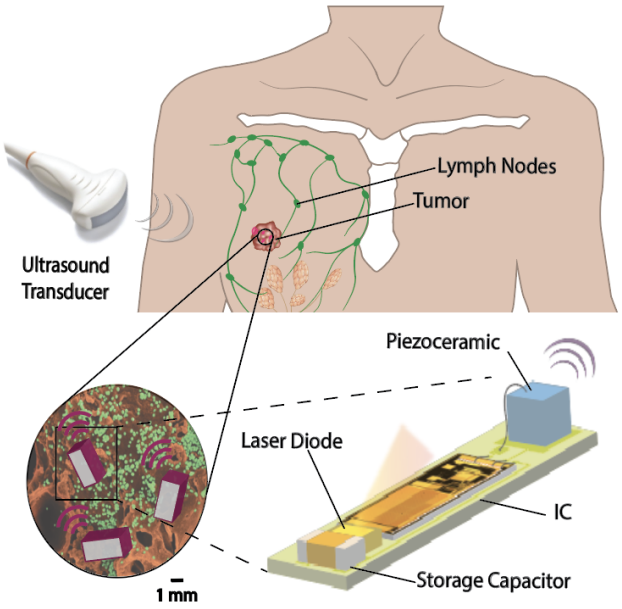

Fig. 1. Concept of an implantable fluorescence imaging system (piezoceramic, imager IC, laser diode and storage capacitor) communicating with an ultrasound transducer

While state-of-the-art chip-scale imagers provide high resolution for multicellular visualizations, they are not implantable inside the body [8]. The fluorescence imagers proposed in [9] and [10] require external wiring for power and data transfer; hence, impractical to be utilized as standalone implants for long-term real-time monitoring. This has led us to propose an implantable fluorescence imager to implement a "wireless biopsy", leveraging new innovations in optics fused with advances in CMOS technology to personalize medication based on the individual response of the patients. Infiltration of the immune cells into the cancerous tissue and disease progression can be assessed by imaging the immune cells and the tumor labeled with fluorescently tagged biomarkers systemically injected in a host of clinical trials [11], [12]. Miniaturization of the implant to the size applicable to implantation via a core biopsy needle (millimeter-scale) imposes stringent limits on the dimensions of the imager. Therefore, in this proposed solution, bulky

R. Rabbani, H. Najafiaghdam, M. M. Ghanbari, B. Zhao, M. Roschelle, V. Stojanovic and R. Muller are with the Department of Electrical Engineering and Computer Sciences, University of California, Berkeley, CA 94720 USA (corresponding author e-mail: rozhan_rabbani@berkeley.edu)

E. Papageorgiou was with the Department of Electrical Engineering and Computer Sciences, University of California, Berkeley, CA 94720 USA.

M. Anwar is with the Department of Radiation Oncology, University of California, San Francisco, CA 94158 USA (e-mail: mekhail.anwar@ucsf.edu)

optics are eliminated to avoid any disruption for implantation and operation of the device [13]. To obviate the need for optical lenses, a fiber optic plate coupled with on-chip optical structures called angle-selective gratings (ASGs) are utilized to restrict the angle of incident light resulting in images with higher resolution [14]. The stand-alone operation of this system on a chip (SoC) miniaturized microscope relies on providing illumination with a mm-sized laser diode as well as wireless power and data transfer controlled by an external interrogator. Inspired by current medical implants, an ultrasonic link is utilized to leverage the low attenuation ($\sim$ 1 dB/cm/MHz) of acoustic waves in the tissue to enable efficient wireless power transmission and communication with a deeply seated imager implant [15], [16].

This manuscript introduces a fully contained proof-of-concept chip-scale imager interfacing with the biological world by detecting small clusters (<1 mm) of fluorescence-labeled cells in real-time and wireless transmission of the data to an external transducer. If deployed inside the body, local networks of implantable imagers can be incorporated for a variety of applications including resolving a 3D structure of the tumor and estimating the depth information from overlaid stacks of the cells. In this paper, we present how the overall system powers up, captures an image from a fluorescent dye, Cyanine5.5-NHS (Cy5.5), converts and transfers the data back to construct the image. Section II discusses system-level design challenges and the corresponding solutions. Section III entails proof-of-concept experimental results of imaging a resolution target with the fluorescent dye, and Section IV concludes the work.

II. Implantable Imaging System

Design of a self-contained implant for fluorescence microscopy relies on integration of the power and data transceiver, the optical illumination source (as light cannot penetrate from an external source deep into the body) and the CMOS imager array. As shown in Fig. 1, the implant consists of: (1) a piezoceramic to harvest power (from acoustic waves launched by a distant external interrogator) and wireless transmission of data through an ultrasound (US) link, (2) the imager IC fused with ASG filters to capture the optical signal generated by (3) the mm-sized laser diode and (4) a storage capacitor. The device can be implanted using core biopsy needles, similar to gold-seed fiducial implants used to mark tumors for radiotherapy [17]. This section describes in detail the strategies to address design challenges for each component and the full system.

A. Fluorescence Microscopy

Prior to imaging, the cells are labeled with fluorophores engineered to conjugate with antibodies specifically targeting the cells of interest. Once bound to the target, the fluorophores are excited by the excitation light resulting in emission of a longer-wavelength light after a Stokes shift [18]. The emitted light is filtered by an optical bandpass filter and is captured by the CMOS sensor. The received

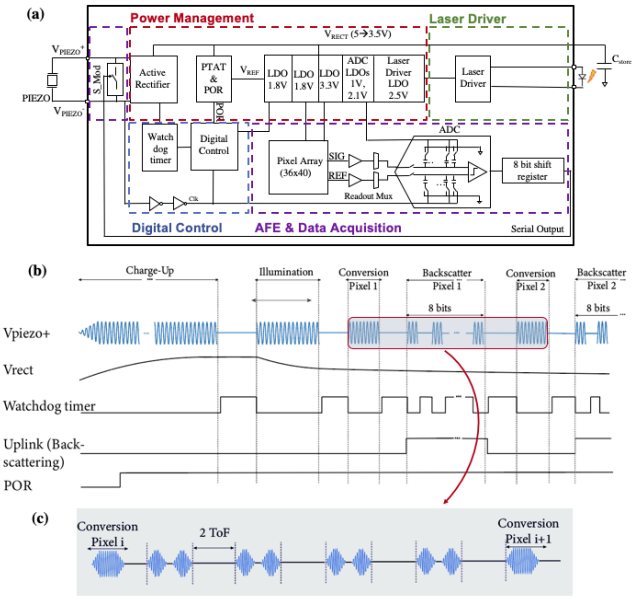

Fig. 2. (a) Circuit block diagram of the IC (b) timing diagram of the Finite State Machine and the corresponding critical signals (c) detailed backscattering protocol

fluorescence signal from a cell is computed as follows

$$F = \sigma Q P_{in} N, \tag{1}$$

where σ is the fluorophore absorption cross section in cm^2, Q is the fluorescence quantum yield, P_{in} is the incident light flux in W/cm^2, and N is the number of fluorophores attached to the cell [19]. A typical Cyanine5.5-NHS Dye that can be excited by a 635 nm laser diode, has quantum yield and fluorophore absorption cross section equal to 20% and 10^{-16} cm^2, respectively [20], [21], therefore, an optical input power close to 30 mW/cm^2 is needed to generate a 200 fW signal that can be detected by the sensor [13].

B. Optical Source

As shown in (1), inefficiency of fluorophores in emitting the received optical power, due to their small absorption cross-section, determines the required optical power for the excitation source to maintain high sensitivity while detecting small clusters of cell foci.

A 635 nm edge-emitting laser diode provides an excitation power close to 30 mW/cm^2 at its nominal operating point. A Stokes shifted longer wavelength photon at 710 nm is emitted, and detected by the imager. A bandpass interference filter (ET 710/55 nm, Chroma) rejects any input light with wavelengths shorter than 682 nm including the excitation light by 60 dB. A 500 µm-thick quartz wafer with a wavelength selective coating is epoxied on top of the chip. To achieve the required incident optical flux, the laser diode is operated with a nominal voltage and current of 2.2 V and 33 mA as shown in Fig. 4(b).

C. CMOS Imager SoC Design

Fig. 2(a) shows the block diagram of our implantable imager, consisting of 4 main blocks: the pixel array, power management unit, laser driver and the Finite State Machine (FSM) for digital control. The chip measuring 2.4 mm by 4.7 mm was fabricated in a standard 0.18µm 1.8V/5V/32V process. Detailed design of the pixel array is presented in [13]. The photodiode current for each pixel in the 36x40 array is integrated on the feedback capacitor of the capacitive transimpedance amplifiers (CTIAs). The output voltage is sampled twice at the beginning and end of the integration time generating reference and signal values respectively. This correlated double sampling (CDS) scheme suppresses offset and low frequency noise. Provided typical values described in Section II.A, 8 integration times ranging from 16 ms to 128 ms in steps of 16ms can be hard-coded for each device. Signal and reference voltages of each pixel are read sequentially, subtracted and converted to a digital signal using a differential 8-bit SAR ADC. The serialized data is backscattered wirelessly using an on-off keying (OOK) modulation scheme to sustain robustness while transferring 11.5 kbit/frame of image data that will be discussed in the next section. The power management unit rectifies the input AC waveform to a 5 V DC voltage to supply the entire SoC. Various on-chip low-dropout voltage regulators (LDOs) regulate the supply voltage (1V, 1.8V, 2.1V, 2.5V, 3.3V) for the imager, the FSM, the laser driver and the ADC. The harvested energy is stored on a 1.4 mF off-chip storage capacitor during US power transfer to get utilized during illumination of the laser diode. The laser driver generates a 50 kHz, 50% duty-cycled pulsed current of 33 mA only during the integration interval. The supply voltage of the laser driver is regulated to 2.5 V to refrain from damaging the laser diode. A dedicated FSM controls co-operation of the imager with the laser driver and is synchronized with a clock signal extracted from the AC signal. Fig. 2(b) depicts timing diagram and state transitions of the chip. The operation of the chip is broken down into 4 states: Charge-Up, Illumination, ADC Operation and Backscattering Modulation. A watchdog signal (triggered in the absence of US pulses) keeps track of the state transitions and data transfer [15]. As noted in Section II.B, power consumption of the implant is dominated by the laser diode. To accommodate the electrical power of 36.3 mW for the laser diode (72.6 mW nominal electrical power with a 50% duty cycle) during illumination, a 1.4 mF storage capacitor is chosen to store charge during power-up. The chip starts harvesting power upon arrival of the incident US input and remains in charge-up state until the rectified voltage (Vrect) reaches 5 V. After the LDO voltages are established, a power-on reset (POR) signal initializes the digital control. During the charge-up state, the pixel array is turned off to speed up the initial charging period. Followed by the illumination state, the first transition of the watchdog signal is indicative of the end of the charge-up period. During illumination, the diode turns on while the photodiode current starts getting integrated for each pixel

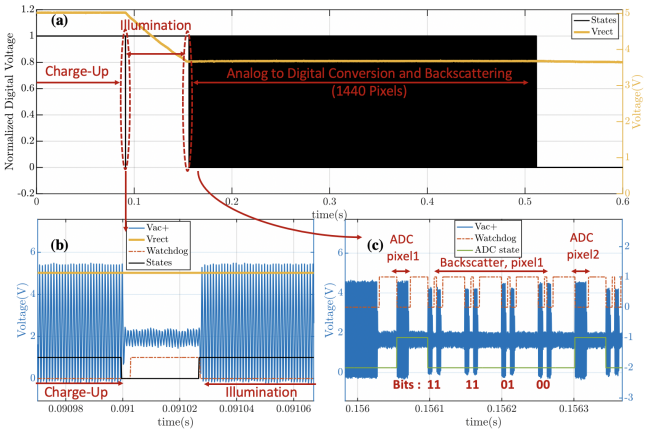

Fig. 3. Measured state transitions (a) FPGA control signal for AM Modulation of the AC source (b) Charge-Up (only the last 90 ms is shown) and Illumination states (c) Analog to digital conversion and backscattering states

and then sampled at the end of the state for subsequent data conversion and backscattering. Power-intensive blocks including the buffers preceding the ADC, the pixel array and the laser driver are duty-cycled off when not being used during data uplink. Despite the considerable droop of Vrect during illumination, the LDOs are designed to operate with input voltages as low as 3.5 V to ensure functionality of the device for the subsequent states. Each pixel's voltage is converted and wirelessly transmitted by modulating the impedance of the same piezoceramic used for power transfer until the watchdog timer counts for the entire 36x40 pixels. The data transfer protocol is discussed in the next part.

D. Wireless Power and Data Transfer Protocols

For low tissue attenuation of acoustic waves while operating in depth inside the body, an US link minimizes the size of the implant and the charge-up period by providing higher power transfer density compared to EM waves and optical links [22], [23]. Maintaining a small form-factor for the implant necessitates having a single-element piezoceramic for both power harvesting and data back-telemetry. Capturing a high resolution image requires transferring 11.5 kbits (34x40=1440 pixels, 8-bit per pixel) per frame. A pulsed-echo OOK modulation scheme is implemented to separate power and data transfer in time domain while using a single piezoceramic for both. A robust backscattering scheme is implemented as shown in Fig. 2(c), where each 8-bit packet is divided into sets of 2 bits fit within the 26.7 us roundtrip (2ToF, time-of-flight) of US waves for a depth of 2 cm. Wireless transmission of a single bit by means of OOK-modulated ultrasound backscattering requires modulation of the termination impedance of the piezo, R_{Load}. At the series resonance frequency, fs, the normalized backscattered echo amplitude is proportional to $R_{Load}/(R_{Load}+R_{piezo})$, where R_{piezo} is the internal resistance of the piezo at fs [24]. Therefore, a modulation switch, S_Mod in Fig. 2(a), is used to modulate R_{Load} and ultimately the echo amplitude for

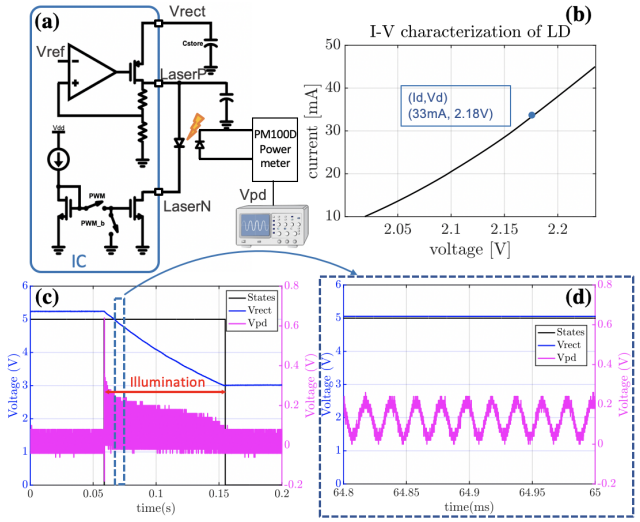

Fig. 4. (a) setup for measuring optical power of the laser diode driven by the on-chip laser driver (b) I-V characterization of the laser diode and its nominal operating point (c) voltage of the photodiode in PM100D power meter during a 96ms illumination interval (d) 50% duty-cycled, 50 kHz photodetector output voltage

OOK modulation.

III. Experimental Results

In this section a proof-of-concept demonstration of the operation of the SoC with a sinusoidal input signal, amplitude modulated (AM) by an FPGA (Xilinx Spartan-6 LX45) is presented. Input frequency and equivalent impedance of the AC source are chosen to replicate the resonance frequency and electrical impedance of a 1.5x1.5x1.5 mm^3 piezoceramic (Lead Zirconate Titanate, PZT) measured in canola oil ($\sim$ 0.25 dB/cm attenuation at 1 MHz). The 1 MHz AC signal is applied as an input voltage source with a series resistance of 2 kΩ to electrically model the piezoceramic. Each IC block is characterized separately and functionality of the entire system is verified by imaging a fluorescent dye Cyanine5.5-NHS, distributed over a resolution test target providing a fine spatial structure to evaluate the image resolution.

A. State Transitions

The required charge-up time for the storage capacitor is characterized by varying the interval the AC signal is applied during the initial state. For a 1.4 mF storage capacitor, Vrect reaches 5 V after 20 s, which enables capturing minute-scale movements of cells inside the tissue environment [25]. State transitions of the IC for a 20 s charge-up, 64 ms illumination and 13.5 us ToF (27 us round-trip interval) are shown in Fig. 3. A digital state control signal from the FPGA modulates the AC signal. Fig. 3 shows the AC input signal and the output of the watchdog timer for a complete set of Charge-Up, Illumination, ADC conversion and Backscattering states. As depicted in Fig. 3(c), the AC signal is modulated by the serialized output of the ADC with a modulation depth of 91%. The amplitude modulated AC signal in Fig. 3(c)

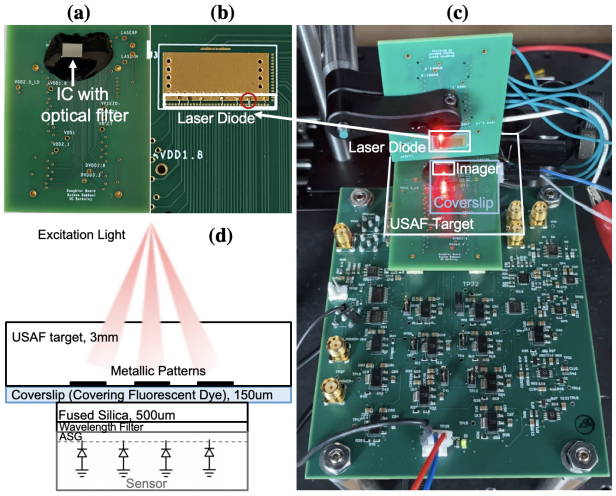

Fig. 5. (a) Imager IC with the optical filter, dark epoxy for optical isolation (b) laser diode mounted and wire-bonded (c) imaging setup for Cy5.5 distributed over the USAF target (d) diagram of the imaging setup

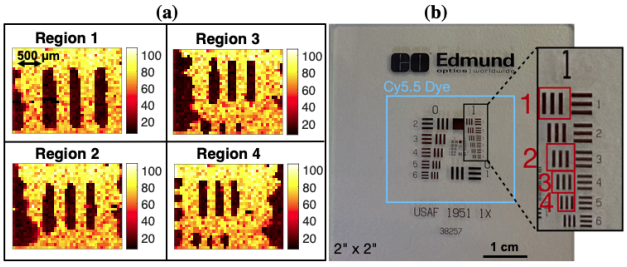

Fig. 6. (a) Images from Cy5.5 dye on 4 regions of the USAF target (pixel values are shown in ADC codes) (b) USAF target with coverslip and the corresponding 4 regions

corresponds to the digitized value of 8'b11110100 for the first pixel with MSB being the first transmitted bit.

B. Optical Power

Fig. 4(a) shows the setup to verify performance of the laser driver. The output optical power of the laser diode is measured using the photodiode voltage output of a power meter (PM100D, Thorlabs) which is proportional to the detected optical power. As shown in Fig. 4(d) the photodiode voltage (Vpd) is a 50 kHz, 50% duty-cycled signal tracking the current applied to the laser diode. Using PIV characterization of the photodiode, the measured laser diode current varies from 33.5 mA to 29 mA corresponding to optical powers of 2.1 mW to 0.9 mW respectively. The 13% current drop stems from the droop in Vrect throughout the illumination state, which can be improved by using a larger storage capacitor.

C. Imaging Setup

Fig. 5 shows the experimental setup for imaging the fluorescent dye on a resolution target. The Chroma ET 710/55nm bandpass filter is epoxied on top of the chip and black epoxy is applied on the wire-bonds covering all sides to avoid any bleed-through from ambient light and the excitation source

as shown in Fig. 5(a). The laser diode is epoxied and wire-bonded to a separate board and connected to output pads of the laser driver in Fig. 5(b). Cyanine5.5-NHS Dye is applied on a coverslip on a USAF 1951 Resolution Target. Each image is captured, converted and streamed out in real-time after a 20 s charge-up interval.

D. Imaging Fluorescent Dyes

Fig. 6(a) shows the output images of the corresponding metallic locations on the USAF target illuminated by the 635 nm Roithner laser diode and emitted from the fluorescent dye. As depicted in Fig. 6(b) the chip captures the selected structures with single pixel resolution ($\sim$ 55 μm) with a 64 ms integration time. This is a proof-of-concept demonstration of the performance of the SoC for a bench-top experimental setup. The input source is applied in a setup representative of the piezoceramic device which facilitates reproducibility for a fully wireless setup imaging ex-vivo samples.

IV. CONCLUSIONS

This work presents a fully-contained implantable image sensor to provide real-time assessments of the tissue at early stages of disease progression addressing challenges in immunotherapy. We demonstrate, to the best of our knowledge, a prototype for unprecedented wireless chip-scale fluorescence microscopy with frame times close to 20-25 s eliminating the need for focusing lenses, fiber optics, batteries or any external wiring.

ACKNOWLEDGMENT

Research reported in this publication was supported by National Institute of Biomedical Imaging and Bioengineering of the National Institutes of Health under award number R21EB027238 and the Office of the Director and the National Institute for Dental and Craniofacial Research of the National Institutes of Health under award number DP2DE030713. The TSMC University Shuttle Program provided CMOS chip fabrication for BSAC (Berkeley Sensors and Actuators Center).

REFERENCES

[1] S. A. Rosenberg, "Shedding Light on Immunotherapy for Cancer," *New England Journal of Medicine*, vol. 350, no. 14, pp. 1461-1463, 2004.

[2] P. Sharma et al., "Primary, Adaptive, and Acquired Resistance to Cancer Immunotherapy," *Cell*, vol. 168, no. 4, pp. 707-723, 2017.

[3] L. A. Emens et al., "Cancer immunotherapy: Opportunities and challenges in the rapidly evolving clinical landscape," *European Journal of Cancer*, vol. 81, pp. 116-129, 2017.

[4] H. L. Kaufman et al., "The Society for Immunotherapy of Cancer consensus statement on tumour immunotherapy for the treatment of cutaneous melanoma," *Nature Reviews Clinical Oncology*, vol. 10, pp. 588–598, 2013.

[5] A. Haslam and V. Prasad, "Estimation of the Percentage of US Patients With Cancer Who Are Eligible for and Respond to Checkpoint Inhibitor Immunotherapy Drugs," *JAMA Network Open*, vol. 2, no. 5, pp. e192535-e192535, May 2019.

[6] E. B. Garon et al., "Five-Year Overall Survival for Patients With Advanced Non–Small-Cell Lung Cancer Treated With Pembrolizumab: Results From the Phase I KEYNOTE-001 Study," *Journal of Clinical Oncology*, vol. 37, no. 28, pp. 2518-2527, 2019.

[7] J. V. Frangioni, "New technologies for human cancer imaging," *Journal of Clinical Oncology*, vol. 26, no. 24, pp. 4012-21, 2008.

[8] R. R. Singh et al., "A CMOS/Thin-Film Fluorescence Contact Imaging Microsystem for DNA Analysis," *IEEE Transactions on Circuits and Systems I: Regular Papers*, vol. 57, no. 5, pp. 1029-1038, May 2010.

[9] Y. Sunaga et al., "Implantable imaging device for brain functional imaging system using flavoprotein fluorescence" *Japanese Journal of Applied Physics* , vol. 55, no. 3S2, 2016.

[10] J. Heymes et al., "Implantable CMOS pixel sensor for positron imaging in rat brain," *Nuclear Instruments and Methods in Physics Research Section A: Accelerators, Spectrometers, Detectors and Associated Equipment*, vol. 911, no. 24, pp. 19-24, 2018.

[11] F. Galli, J. V. Aguilera, B. Palermo et al., "Relevance of immune cell and tumor microenvironment imaging in the new era of immunotherapy," *Journal of Experimental & Clinical Cancer Research*, vol. 39, 2020.

[12] L. Ye et al., "Tumor-Infiltrating Immune Cells Act as a Marker for Prognosis in Colorectal Cancer," *Frontiers in Immunology*, vol. 10, pp. 2368, 2019.

[13] E. P. Papageorgiou, B. E. Boser and M. Anwar, "Chip-Scale Angle-Selective Imager for In Vivo Microscopic Cancer Detection," *IEEE Transactions on Biomedical Circuits and Systems*, vol. 14, no. 1, pp. 91-103, 2020.

[14] E. P. Papageorgiou, B. E. Boser and M. Anwar, "Chip-scale fluorescence imager for in vivo microscopic cancer detection," *2017 Symposium on VLSI Circuits*, 2017, pp. C106-C107.

[15] D. K. Piech, B. C. Johnson and K. Shen et al., "A wireless millimetre-scale implantable neural stimulator with ultrasonically powered bidirectional communication," *Nature Biomedical Engineering*, vol. 4, pp. 207–222, 2020.

[16] M. J. Weber et al., "A Miniaturized Single-Transducer Implantable Pressure Sensor With Time-Multiplexed Ultrasonic Data and Power Links," *IEEE Journal of Solid-State Circuits*, vol. 53, no. 1, pp. 1089-1101, 2018.

[17] S. Akram et al., "Transperineal implantation of gold fiducial markers (gold seeds) for prostate image-guided radiation therapy: a feasible technique associated with a low risk of complications," *Journal of medical radiation sciences*, vol. 62, pp. 261-266, 2015.

[18] K. Ito et al., "Near-Infrared Photochemoimmunotherapy by Photoactivatable Bifunctional Antibody–Drug Conjugates Targeting Human Epidermal Growth Factor Receptor 2 Positive Cancer," *Bioconjugate Chemistry*, vol. 28, no. 5, pp. 1458-1469, 2017.

[19] M. A. Albota, C. Xu, and W. W. Webb "Two-Photon Fluorescence Excitation Cross Sections of Biomolecular Probes from 690 to 960 nm," *Applied Optics*, vol. 37, pp. 7352-7356, 1998.

[20] L. Wang, A. K. Gaigalas and V. Reipa, "Optical properties of Alexa 488 and Cy5 immobilized on a glass surface," *Biotechniques*, vol. 38, no. 1, pp. 127-32, Jan 2005.

[21] G. Hong et al., "Near-Infrared-Fluorescence-Enhanced Molecular Imaging of Live Cells on Gold Substrates," *Angewandte Chemie International Edition*, vol. 50, no. 20, pp. 4644-4648, 2011.

[22] J. Thimot, K. L. Shepard "Bioelectronic devices: Wirelessly powered implants," *Nature Biomedical Engineering*, vol. 1, Nov. 2017.

[23] S. Ayazian and A. Hassibi, "Delivering optical power to subcutaneous implanted devices," *2011 Annual International Conference of the IEEE Engineering in Medicine and Biology Society*, 2011, pp. 2874-2877.

[24] M. M. Ghanbari and R. Muller, "Optimizing Volumetric Efficiency and Backscatter Communication in Biosensing Ultrasonic Implants," *IEEE Transactions on Biomedical Circuits and Systems*, vol. 14, no. 6, pp. 1381-1392, Dec. 2020.

[25] S. Qi et al., "Long-term intravital imaging of the multicolor-coded tumor microenvironment during combination immunotherapy," *eLife*, vol. 5, pp. e14756, Nov. 2016.